

See discussions, stats, and author profiles for this publication at: <https://www.researchgate.net/publication/261564213>

Theoretical studies on benzimidazole and imidazo[1,2-a]pyridine derivatives as Polo-like kinase 1 (Plk1) inhibitors: Pharmacophore modeling, atom-based 3D-QSAR and molecular dockin...

ARTICLE *in* JOURNAL OF SAUDI CHEMICAL SOCIETY · APRIL 2014

Impact Factor: 2.52 · DOI: 10.1016/j.jscs.2014.03.007

CITATION

1

READS

32

5 AUTHORS, INCLUDING:



Naresh Kandakatla

Sathyabama University

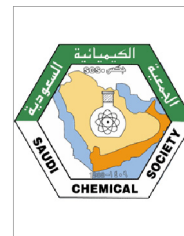
15 PUBLICATIONS 9 CITATIONS

SEE PROFILE



King Saud University
Journal of Saudi Chemical Society

www.ksu.edu.sa
www.sciencedirect.com



ORIGINAL ARTICLE

Theoretical studies on benzimidazole and imidazo[1,2-a]pyridine derivatives as Polo-like kinase 1 (Plk1) inhibitors: Pharmacophore modeling, atom-based 3D-QSAR and molecular docking approach

Rajasekhar Chekkara ^{a,b,*}, Naresh Kandakatla ^a, Venkata Reddy Gorla ^{a,c},
Sobha Rani Tenkayala ^{a,c}, E Susithra ^d

^a Department of Chemistry, Sathyabama University, Jeppiaar Nagar, Chennai 600119, India

^b GVK Biosciences Pvt. Ltd., Plot No: 79, IDA-Mallapur, Hyderabad 500076, India

^c Department of Chemistry, Dravidian University, Srinivasavanam, Kuppam 517426, India

^d Department of Pharmacy, Sri Ramachandra University, Porur, Chennai 600116, India

Received 20 November 2013; revised 12 March 2014; accepted 21 March 2014

KEYWORDS

Polo-like kinase 1;
Pharmacophore modeling;
3D-QSAR;
Docking;
Benzimidazole;
Imidazo[1,2-a]pyridines

Abstract Molecular modeling studies were carried out on a series of benzimidazole and imidazo[1,2-a]pyridines as Plk1 inhibitors. Based on the pharmacophore model, we obtained a five-featured hypothesis AADRR, with two hydrogen bond acceptors, one hydrogen bond donor and two aromatic rings. An atom-based 3D-QSAR model was predicted for 36 training set ($R^2 = 0.9475$, $SD = 0.1927$, $F = 99.3$) and nine test set ($Q^2 = 0.6519$, $RMSE = 0.4044$, Pearson $R = 0.834$) compounds using a pharmacophore-based alignment. From these results, AADRR pharmacophore feature was chosen as the best common pharmacophore hypothesis, whereas the atom-based 3D-QSAR results explain the importance of hydrophobic and electron-withdrawing features for the most active compound 32. The dataset molecules were docked into the active site of Plk1, which shows acceptable hydrogen bond interactions with residues Cys133, Asp194, Glu131, Lys82 and Glu140 and also shows further hydrogen bond interactions with hydrophobic residues Cys67, Leu59 and Arg136. These results can be helpful for further design of novel Plk1 inhibitors.

© 2014 King Saud University All rights reserved.

* Corresponding author at: Department of Chemistry, Sathyabama University, Jeppiaar Nagar, Chennai 600119, India. Tel.: +044 24500646.

E-mail address: chekkara.rajasekhar@gmail.com (R. Chekkara).

Peer review under responsibility of King Saud University.



Production and hosting by Elsevier

1. Introduction

Polo-like kinases (Plks) are a family of serine/threonine kinases critical for all stages of cell cycle progression, specifically mitosis [1]. Of the different human Plks identified so far viz. Plk 1 (Plk), Plk2 (Snk), Plk3 (Fnk/Prk), Plk4 (Sak) and Plk5, Plk 5 may not be involved in cell cycle progression, probably due to the lack of the kinase domain [2,3,4]. Typically, all Plks

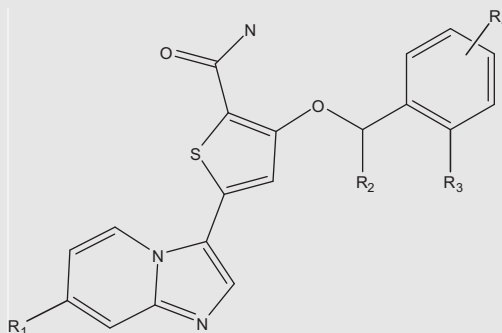
contain an N-terminal catalytic kinase domain which is responsible for enzyme activation and ATP-binding and a C-terminal region that consists of one or two polo box domains (PBDs) involved in phosphopeptide binding. Plk1, the best characterized member of the Plk family [5,6] regulates several key steps in the pathway of cells through G2/M transition, centrosome maturation, early embryonic development, DNA replication, kinetochore assembly, bipolar spindle formation and cytokinesis [7,8,9,10,11,12,14,15]. All these Plk1 activities are associated with its subcellular localization. In interphase (G₁, S, G₂), Plk1 is involved in DNA replication and centrosome maturation [13,14], in prophase to mitotic entry [15,16], in prometaphase and metaphase, Plk1 might be involved in spindle assembly/formation and at telephase, it acts as a key regulator of cytokinesis [17]. Hence, downregulation of Plk1 activity promotes cell cycle arrest and apoptosis [18,19].

Over expression of Plk1 is observed in a broad spectrum of cancer types [20,21,22,23,24,25], and its expression often correlates with the prognosis of tumor patients. A wide range of natural and synthetic drugs, nearly 20–30 molecules are present

in clinical and preclinical stage development [26]. Depending on the oncogenic transformation potential of the enzyme, small molecular inhibition of Plk1 enzymatic activity by blocking its catalytic domain became a momentous feature in cancer therapy [27,28,29,30].

The aim of this study is to generate a 3D pharmacophore model, an atom based 3D-QSAR and molecular docking studies of known Plk1 inhibitors, to know the molecular mechanisms and structural requirements significantly to the Plk1 inhibition and for further molecular design of potent novel inhibitors of Plk1. A Pharmacophore model was generated, which illustrates the importance of specific structural features, like the nature of atoms, hydrophobicity, the functional groups and aromatic features of molecules targeted for a particular enzyme [31,32]. An atom-based 3D-QSAR model was also developed for understanding the structure–activity relationship of a set of molecules using PHASE [33]. The binding mode and the intermolecular interactions between ligands and the Plk1 enzyme were examined by performing LigandFit module of Discovery Studio 2.5.

Table 1 Chemical structures of the training and test set molecules 1–18.



Compound	R ₁	R ²	R ₃	R ₄
1	H	H	CF ₃	H
2	H	Me(R)	CH ₂ OH	H
3	H	Me	Cl	5-CH ₂ OH
4	H	Me(R)	Cl	4-CH ₂ OH
5	CH ₂ OH	Me(R)	Cl	H
6	CH ₂ OH	Me	Cl	H
7	H	Me(R)	Cl	4-(<i>i</i> -Propylamino)methyl
8	H	Me(R)	Cl	4-(<i>c</i> -Propylamino)methyl
9	H	Me(R)	Cl	4-(<i>c</i> -Pentylamino)methyl
10	H	Me(R)	Cl	4-(2-Hydroxyethylamino)methyl
11	H	Me(R)	Cl	4-(3-Hydroxypropylamino)methyl
12	H	Me(R)	Cl	4-(1-Hydroxy-2-methylpropan-2-ylamino)methyl
13	H	Me(R)	Cl	4-(4-Fluoropiperidin-1-yl)methyl
14	H	Me(R)	Cl	4-(4-Methylpiperazin-1-yl)methyl
15	H	Me(R)	Cl	4-(4-Hydroxypiperidin-1-yl)methyl
16	H	Me(R)	Cl	
17	H	Me(R)	Cl	4-(<i>tert</i> -butylamino)methyl
18	H	Me(R)	CF ₂ H	4-(<i>tert</i> -butylamino)methyl

2. Computational methods

2.1. Dataset

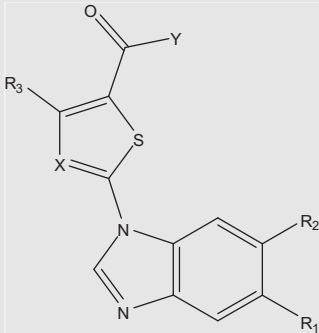
The dataset of 45 benzimidazole and imidazo[1,2-a] pyridine derivatives having Plk1 inhibitory activity was used for 3D-QSAR study as shown in Tables 1 and 2 [34–38]. The inhibitory concentration (IC₅₀) of the Plk1 inhibitors was converted into pIC₅₀ (pIC₅₀ = –logIC₅₀). The compounds in the data set were divided randomly into 80% of training set and 20% of test set molecules. Thirty-six molecules of the training test were used for the generation of pharmacophore

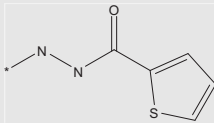
models, nine molecules of the test set for validation of the proposed models and for prediction of the activity.

2.2. Ligand preparation

LigPrep module (v2.3 Schrödinger 2009) [39], was used for hydrogen addition, to convert the 2D structures to 3D and for energy minimization of ligands using OPLS-2005 as a force field. Tautomeric forms were generated using Macro-Model method (v9.7, Schrödinger 2009) [40] after discarding the current conformers. Mixed MCMM/LMOD Search Method was used for conformer generation with OPLS-

Table 2 Chemical structures of the training and test set molecules 19–45.



Compound	R ₁	R ₂	X	Y	R ₃
19	OMe	OMe	CH	NH ₂	1(S)-(2-chlorophenyl)ethoxy
20	H	H	CH	NH ₂	2-(Trifluoromethyl)benzyloxy
21	OMe	OMe	N	OH	3,5-Dichlorophenyl
22	OMe	OMe	N	OH	(3-Bromophenyl)
23	OMe	OMe	N	OH	3-(Trifluoromethyl)phenyl
24	OMe	OMe	N	OH	3-Chloro-4-(trifluoromethyl)phenyl
25	OMe	OMe	N	OH	1-Methyl-1H-indol-5-yl
26	OMe	OMe	N	OH	3,4-Difluorophenyl
27	2-Methoxyethoxy	2-Methoxyethoxy	N	OH	Phenyl
28	OMe	OMe	N	OH	3-(Hydroxymethyl)phenyl
29	OMe	OMe	N	OH	2,3-Dihydrobenzo[b][1,4]dioxin-6-yl
30	OMe	OMe	N	OH	4-Vinylphenyl
31	OMe	OMe	N		3-Chlorophenyl
32	Phenyl	H	CH	NH ₂	1(R)-(2-(trifluoromethyl)phenyl)ethoxy
33	H	Phenyl	CH	NH ₂	1(R)-(2-(trifluoromethyl)phenyl)ethoxy
34	H	2-Chloropyridin-4-yl	CH	NH ₂	1(R)-(2-(trifluoromethyl)phenyl)ethoxy
35	2-(Piperazin-1-yl)pyridin-4-yl	H	CH	NH ₂	1(R)-(2-chlorophenyl)ethoxy
36	H	Piperidin-4-yloxy	N	NH ₂	3-Chlorophenyl
37	H	Cyclohexyloxy	N	NH ₂	3-Chlorophenyl
38	H	2-Morpholinoethoxy	N	NH ₂	3-Chlorophenyl
39	H	3-Morpholinopropoxy	N	NH ₂	3-Chlorophenyl
40	H	3-(Dimethylamino)propoxy	N	NH ₂	3-Chlorophenyl
41	H	3-(4-Methylpiperazin-1-yl)propoxy	N	NH ₂	3-Chlorophenyl
42	OMe	3-(4-Methylpiperazin-1-yl)propoxy	N	NH ₂	3-Chlorophenyl
43	H	(4-Methylpiperazin-1-yl)methyl	N	NH ₂	4-(Trifluoromethyl)phenyl
44	H	(4-Methylpiperazin-1-yl)methyl	N	NH ₂	3-(Trifluoromethyl)phenyl
45*	OMe	OMe	CH	NH ₂	2-(Trifluoromethyl)benzyloxy

* Reference compound GW843682X.

2005 force field and distance-dependent dielectric solvent model as MCMM was found to be a better choice for detailed studies of a relatively less number of compounds or small libraries [41]. For each ligand, a maximum of 2000 conformers were generated ensuring that all the conformers were minimized up to 500 iterations using TNCG minimization. Each minimized conformer was filtered through a relative energy difference window of 10 kcal/mol and RMSD of 1.00 Å.

2.3. Pharmacophore studies

To find the common pharmacophore hypothesis, the data set was divided into active and inactive sets in order to simplify the results of pharmacophore generation and validation.

2.4. Generation of pharmacophore sites

PHASE (v3.1, Schrödinger 2009) [42] identifies the spatial arrangements of functional groups that are common and essential to the biological activity of a set of high affinity ligands. A default six built-in pharmacophore features namely hydrogen bond acceptor (A), hydrogen bond donor (D), hydrophobic group (H), negatively charged group (N), positively charged group (P) and aromatic ring (R) were used to create pharmacophore sites. The salient pharmacophoric features were explained by a set of chemical structure patterns. The assigned structural patterns are specified as SMARTS queries, which allow one of three possible geometries – point, vector and group, representing the physical characteristics of the site. Confirming the activity thresholds as 8.1 and 7.0,

the dataset was divided into five active and fifteen inactive compounds that are to be used for pharmacophore modeling and subsequent scoring.

2.5. Finding common pharmacophore and scoring hypotheses

After comprehensive examination of the pharmacophores, those pharmacophores that are having identical sets of features with very similar spatial arrangements were grouped together. If a given group is retained at least one pharmacophore from each ligand, that group ride as a common pharmacophore. A tree-based partitioning algorithm was used for identification of the common pharmacophores, with a maximum tree depth of five and the Intersite distance was 2 Å. The final size of the pharmacophore box, which governs the tolerance on matching, was 1 Å. Therefore, any pharmacophore in the group could ultimately become a common pharmacophore hypothesis (CPHs).

2.6. Generation of 3D-QSAR model

PHASE presents atom-based or pharmacophore based 3D-QSAR models. Due to a common structural framework of the dataset [43], we have chosen an atom-based 3D-QSAR model to predict the structure–activity relationship (SAR) of the molecules. Atom-based 3D-QSAR models were generated for selected common pharmacophore hypothesis using 36-members of the training set and a grid spacing of 1.0 Å, a random seed value of zero and six PLS factors. The developed 3D-QSAR models were validated by predicting activities of nine test set molecules.

Table 3 Predicted activity and fitness for the training and test sets of compounds.

Compound	Experimental pIC50	Predicted activity	Fitness score	Compound	Experimental pIC50	Predicted activity	Fitness score
1	7.6575	7.66	2.56	24	6.45	6.52	1.58
2	7.0555	7.12	2.67	25	6.4341	6.26	1.68
3	7.4089	7.5	2.6	26 ^a	6.266	6.6	1.69
4 ^b	8.3098	8.02	2.59	27	6.0867	6.05	1.73
5 ^c	8.1366	7.71	2.6	28 ^a	5.9665	6.68	1.69
6 ^a	7.0362	7.69	2.67	29	5.6307	5.74	1.68
7	7.5528	7.63	2.55	30	5.5728	6.24	1.69
8	7.9208	8.01	2.55	31	7.7447	7.83	0.8
9 ^a	7.602	7.64	2.52	32 ^b	8.2218	8.16	3
10	7.6777	7.73	2.54	33	7.7447	7.65	2.62
11	7.7212	7.72	2.53	34	8.3979	8.37	2.67
12	7.6382	7.64	2.52	35	7.2757	7.01	2.73
13 ^a	7.886	7.71	2.51	36	7.0969	7.04	1.74
14 ^b	7.7695	7.81	2.51	37	6.1804	6.19	1.74
15	7.5686	7.7	2.51	38	6.7798	6.73	1.01
16	7.7958	7.85	2.49	39	7.6777	7.68	0.87
17	7.3372	7.36	2.53	40	6.7931	6.64	0.27
18 ^a	7.6989	7.57	2.59	41	7.4948	7.33	0.35
19	7.5228	7.65	2.65	42	7.7212	7.91	0.97
20 ^a	7.4559	7.67	2.31	43	6.1797	6.26	1.43
21 ^a	7.1804	6.79	1.68	44	7.2291	7.32	1.43
22	7.3979	6.82	1.69	45 ^b	8.6575	8.56	2.66
23	6.8041	6.78	1.68				

^a Test set compounds.

^b Pharmset active compounds.

^c Test set and pharmset active compounds.

Table 4 PLS statistical parameters for the best CPHs.

	AADRR	AAARR
SD	0.1927	0.1868
R^2	0.9475	0.9507
F	99.3	106
P	1.111e-019	3.995e-020
RMSE	0.4044	0.403
Q^2	0.6519	0.6542
Pearson R	0.834	0.8175

SD, Standard deviation of the regression; R^2 , correlation coefficient; F , variance ratio; P , significance level of variance ratio; RMSE, root mean-square error; Q^2 , predictive coefficient of the test set; Pearson R , Correlation between the predicted and observed activities for the test set.

2.7. Molecular docking studies

Molecular docking studies were carried out using LigandFit module incorporated in Discovery Studio v2.5 [45]. Usually, the LigandFit docking process includes three stages: (I) Docking of a ligand into a user defined binding site, (II) In-situ ligand minimization, (III) Scoring function calculations for each pose of ligands. The X-ray crystal structure of the Plk1 protein with coordinating complex Plk1-NMS P937 (PDB ID: 2YAC) [44] was obtained from the protein data bank and further modified for LigandFit docking calculations.

Receptor-Ligand interactions panel was used for protein preparation; the water molecules and co-crystallized ligands were removed from the protein and further minimization was performed by applying the CHARMM as force field. The docking energy grid was developed with the co-crystallized ligand NMS-P937 of 2YAC as the center of the grid, the dataset and the newly designed molecules were docked in the active site region of 2YAC using LigandFit of DS to predict the binding interactions between ligands and Plk1 molecule.

3. Results and discussion

A 3D ligand-based pharmacophore model and an atom-based 3D-QSAR model were generated for a set of benzimidazole and imidazo[1,2-a]pyridine derivatives, to understand the effect of spatial arrangement of structural features on Plk1 inhibition. Molecular docking studies were performed to understand the binding mode of ligands against Plk1 protein. Predicted activity and fitness score for the training and test set compounds are shown in Table 3.

The common pharmacophore hypotheses (CPHs) were generated by dividing the dataset into five active molecules ($pIC_{50} \geq 8.10$) and fifteen inactive molecules ($pIC_{50} \leq 7.00$) and on consideration of the rest of the molecule as moderately active. Five featured CPHs were generated with different combinations of variants. On applying the scoring function using default values, two best CPHs,

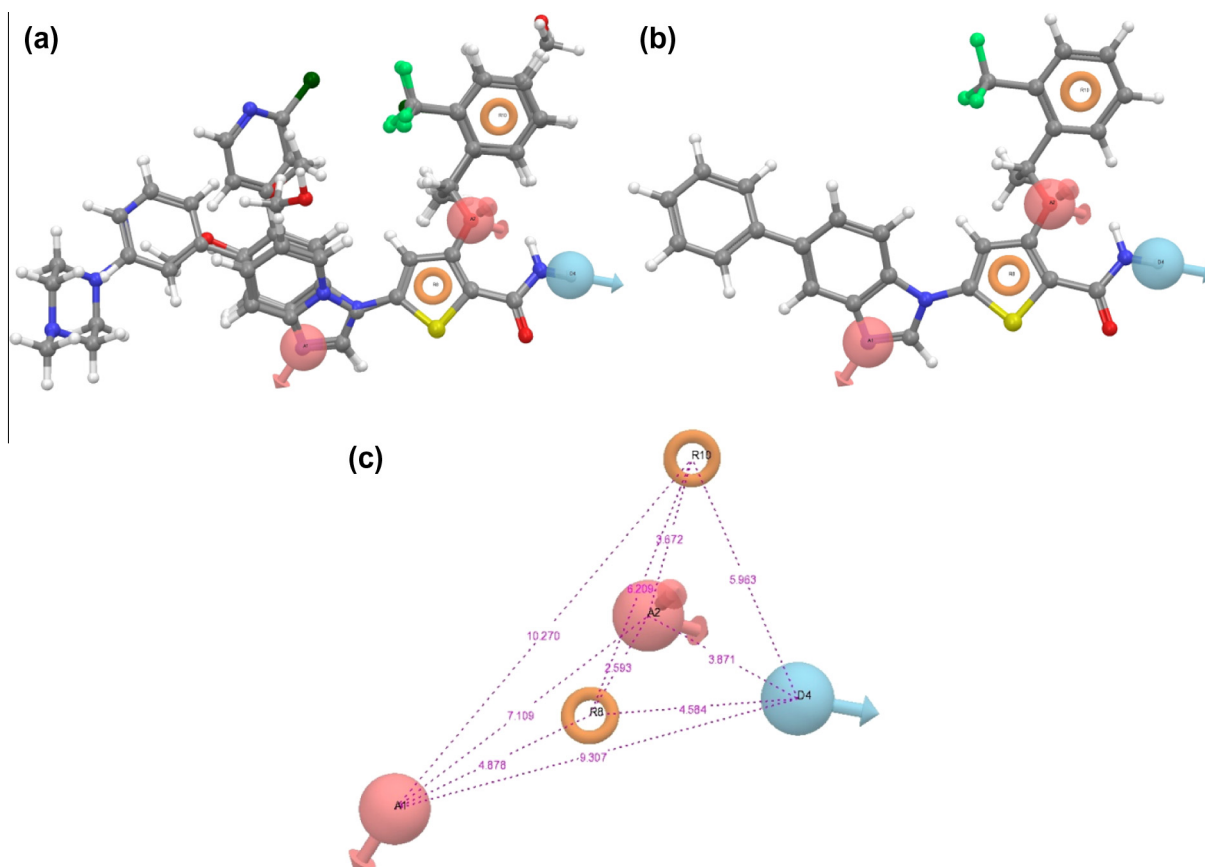


Figure 1 The best AADRR hypothesis model. (a) Alignment of the most active compounds applied to the AADRR hypothesis. (b) Alignment of the most active compound 32 (highest fitness value = 3) applied to the AADRR hypothesis. (c) Hypothesis AADRR, all distances stated in Å.

AADRR and AAARR were selected for the atom-based 3D-QSAR model. The 3D-QSAR models were generated in PHASE using nine test set molecules with six PLS factors. A summary of statistical data for the two best CPHs is listed in the Table 4.

The statistical parameters R^2 , Q^2 , SD, RMSE, Pearson R and F were used for evaluation of the two 3D-QSAR models. AADRR hypothesis has an R^2 value of 0.9475 for the training set and an alluring predictive potential with a Q^2 value of 0.6519 for the test set and when compared with the AAARR hypothesis, AADRR hypothesis possesses a minimum P value of 1.111e-019 and maximum Pearson R value of 0.834. Thus, AADRR (two hydrogen bond acceptors (A), one hydrogen bond donor (D) and two aromatic rings (R) hypothesis was finalized as the best model of CPHs.

The alignment generated by the AADRR hypothesis applied for QSAR model generation is shown in Fig. 1. The correlation between actual and predicted pIC50 of training and test set compounds is shown in Fig. 2. Angles between the different sites of AADRR hypothesis is shown in Table 5.

3.1. QSAR visualization

The contour cubes retrieved from the AADRR hypothesis by 3D-QSAR technique describes the features, which are essential for the interactions between ligand and Plk1 protein. In a comparison of favorable (blue cubes) and unfavorable (red cubes) regions, a visual image of the contours generated for the most active compound 32 is shown in Fig. 3. The cubical representation of different properties such as hydrophobic, electron withdrawing, hydrogen bond donor and combined effect of the most active compound 32 with AADRR hypothesis is shown in Fig. 3a–d.

Visual representation of Fig. 3a shows the presence of blue cubes at A1, A2 and 1-N of the benzimidazole group and at the carboxamide group attached to thiophene ring which shows the favorable regions of electron withdrawing features of the molecules. It can be suggested that the addition of suitable electron withdrawing groups in this favored region will enhance the Plk1 inhibition activity. Fig. 3b describes that the addition of hydrophobic groups at R8, R10, attachment

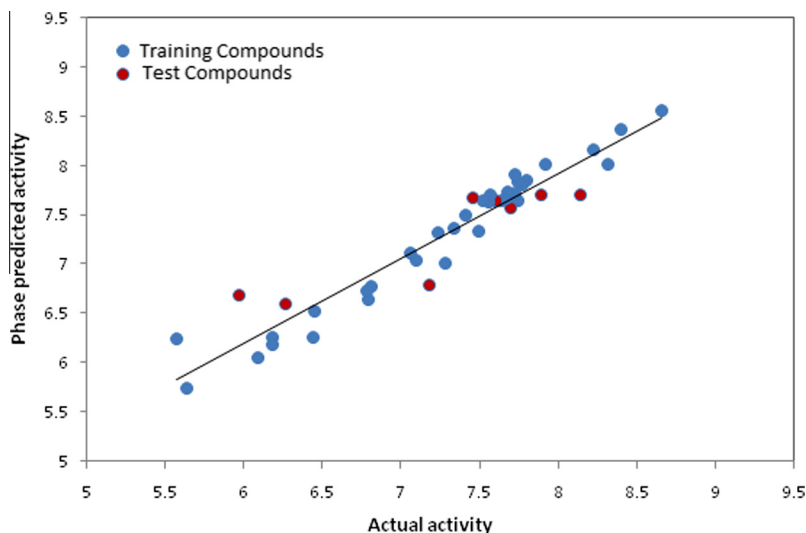


Figure 2 Scatter plot for the predicted and actual pIC50 values of the QSAR model applied to training and test sets.

Table 5 The angles between different sites of AADRR hypothesis.

Site1	Site2	Site3	Angle (°)	Site1	Site2	Site3	Angle (°)
A2	A1	D4	22.6	A2	D4	R8	34.4
A2	A1	R8	12.9	A2	D4	R10	36.6
A2	A1	R10	12.5	R8	D4	R10	70.8
D4	A1	R8	10.1	A1	R8	A2	142.3
D4	A1	R10	35	A1	R8	D4	159.2
R8	A1	R10	25.1	A1	R8	R10	135.4
A1	A2	D4	112.5	A2	R8	D4	57.6
A1	A2	R8	24.8	A2	R8	R10	9.1
A1	A2	R10	142.6	D4	R8	R10	65.1
D4	A2	R8	88	A1	R10	A2	24.9
D4	A2	R10	104.5	A1	R10	D4	63.6
R8	A2	R10	164.4	A1	R10	R8	19.5
A1	D4	A2	44.9	A2	R10	D4	38.9
A1	D4	R8	10.7	A2	R10	R8	6.4
A1	D4	R10	81.4	D4	R10	R8	44.2

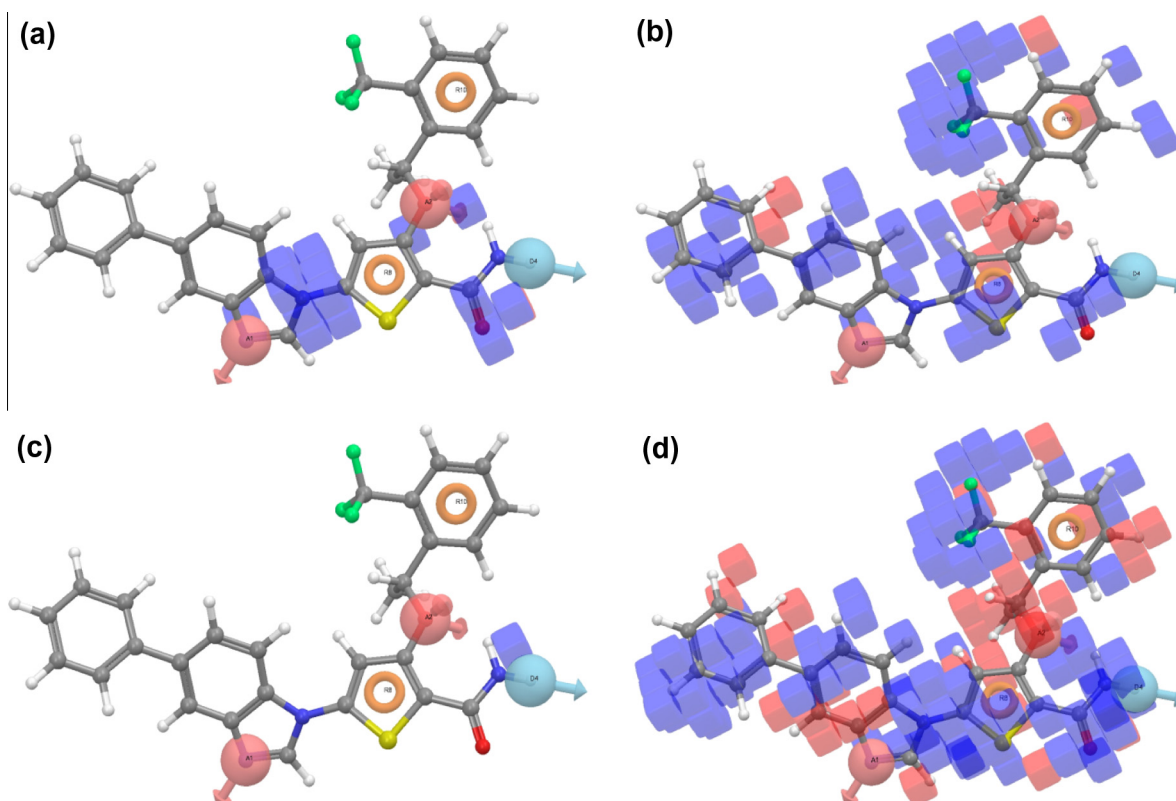


Figure 3 3D-QSAR visualization of various substituents effects; (a) electron withdrawing feature; (b) hydrophobic features; (c) hydrogen-bond donor and (d) combined effect.

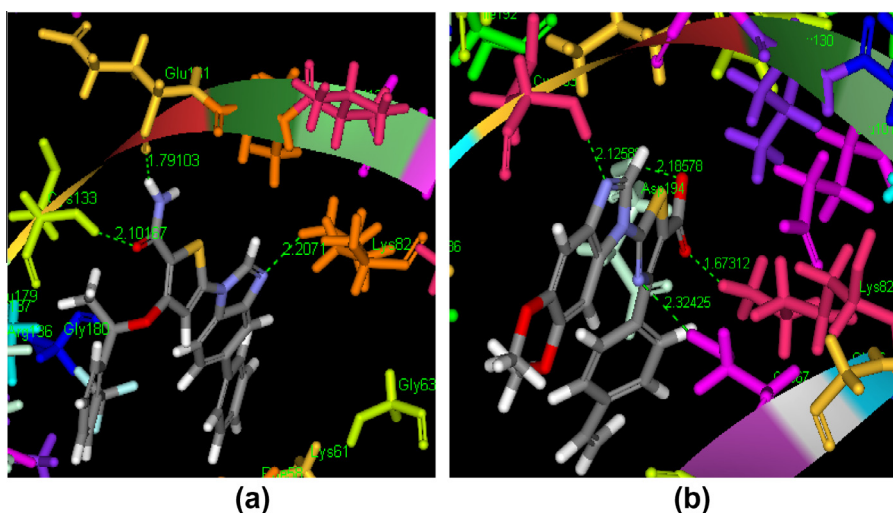
Table 6 LigandFit dock results of the dataset molecules with 2YAC.

Compound	Dock score (kcal/mol)	H-bonds	Interacting amino acids
1	51.652	2	Cys67, Glu140
2	43.868	2	Cys67, Cys133
3	46.575	4	Asp194, Ser137, Gly180, Lys82
4	49.014	4	Arg57, Lys82, Glu131, Cys133
5	54.15	2	Cys67, Glu140(2)
6	48.479	3	Cys67, Cys133, Asp194
7	40.03	2	Gly62, Lys82 (2)
8	39.748	3	Glu140, Asp194, Asn181
9	42.124	5	Lys61, Leu59, Asp194, Lys62, Cys67
10	60.792	3	Asp194, Asn181, Cys133
11	54.433	3	Arg134, Arg57, Cys67
12	30.55	3	Asp194, Asn181, Cys133
13	27.908	3	Cys67, Phe58, Arg57
14	43.302	2	Asp194, Arg136
15	35.318	2	Lys82, Glu140
16	40.442	2	Arg57, Cys67
17	40.341	3	Asp194 (2), Asp181, Glu140
18	17.709	2	Cys67, Leu59
19	45.102	3	Lys82, Asp194, Cys67
20	56.951	3	Lys82, Glu131, Cys133
21	88.276	3	Val128, Cys133, Asp194
22	93.871	3	Lys82, Asp194, Cys133
23	68.983	3	Gly180, Cys67, Arg136 (2)
24	77.042	3	Asp194, Cys67 (2), Arg136
25	75.873	3	Lys82, Cys67, Cys133
26	88.337	3	Lys82 (2), Lys178 (2), Glu140 (2)
27	94.484	3	Lys82, Asp194, Cys133
28	91.231	3	Asp194, Asn181, Lys82

(continued on next page)

Table 6 LigandFit dock results of the dataset molecules with 2YAC.

Compound	Dock score (kcal/mol)	H-bonds	Interacting amino acids
29	85.965	3	Lys82 (2), Cys67, Cys133
30	89.95	4	Asp194, Lys82, Cys67, Cys133
31	64.271	4	Lys61, Cys67, Leu59, Arg57
32	45.317	3	Lys82, Cys133, Glu131
33	45.794	2	Cys67, Glu140
34	47.966	2	Cys133, Lys82
35	55.425	2	Lys178, Asp94 (2)
36	77.503	2	Cys67, Lys178, Glu140 (2)
37	57.272	2	Glu140, Cys67
38	61.966	4	Asp194, Lys82, Cys67, Gly62
39	56.895	3	Asp194, Cys67, Arg136
40	69.444	4	Asp194, Cys67, Cys133, Leu59
41	53.823	3	Lys178, Arg136, Arg57
42	63.543	4	Glu140, Cys67, Asp194, Lys178
43	64.406	5	Cys67, Gly62, Gly196, Gly63, Phe195
44	57.018	3	Glu140, Asp194, Arg57
45	54.369	3	Asp194, Cys67, Glu140

**Figure 4** The docking results of the most active and least active compound; (a) the binding mode of the most active compound 32 (highest fitness score = 3); (b) the binding mode of the least inactive compound 30.

of carboxamide group to the thiophene ring, benzimidazole ring, and phenyl group to the benzimidazole ring, were found to be acceptable and increases the inhibition of the Plk1 activity, whereas the addition of hydrophobic groups near to the ethoxy group attached to thiophene ring decreases the inhibitory potential of the compound represented by the red cubes specifying the negative potential of hydrophobic groups to that particular place. Fig. 3c represents that the blue cubes at the D4 region indicate the positive potential of H-bond donor groups at that position in molecules. Fig. 3d illustrates the combined effect of all features expressing the presence of carboxamide group attached to thiophene ring and benzimidazole ring as favorable regions for Plk1 protein binding.

3.2. Docking analysis

Molecular docking simulations were performed using LigandFit module of DS to understand the binding mode of benz-

imidazole and imidazo[1,2-a]pyridine derivatives against Plk1. In validating the LigandFit dock program, the protein

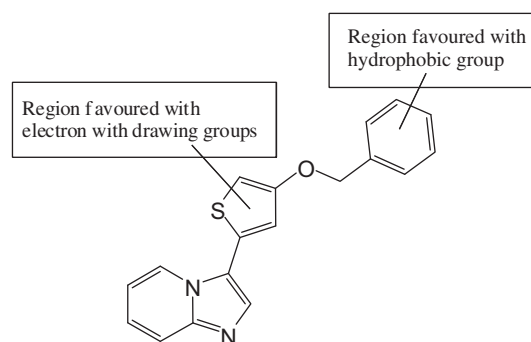
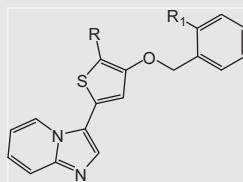
**Figure 5** Structural requirements for binding and inhibitory activity of inhibitors.

Table 7 Structure and docking score of the newly designed molecules.

Comp.	R	R ₁	Docking score (kcal/mol)	H-bonds	Interacting amino acids
D1	-COOH	Me	75.335	2	Lys82, Lys67
D2	-OH	Me	50.118	3	Cys133, Glu131, Lys82
D3	-NO ₂	Me	51.193	3	Lys82, Lys67, Lys178
D4	CF ₃	Me	49.844	2	Cys133, Cys67
D5	OMe	Me	59.641	2	Cys67, Glu140
D6	Ac	Me	49.945	1	Cys67
D12	-COOH	Ph	88.76	2	Cys67, Lys82
D13	-OH	Ph	54.438	2	Asp194, Glu140
D14	-NO ₂	Ph	55.195	3	Lys82, Cys67, Lys178
D15	CF ₃	Ph	44.548	1	Cys133
D16	OMe	Ph	50.425	2	Cys67, Asp194
D17	Ac	Ph	54.414	1	Cys133
D7		Me	54.767	1	Gly180
D8		Me	79.847	2	Asp194, Cys67
D9		Me	51.689	2	Arg57, Glu131
D10		Me	87.384	2	Cys67, Arg57
D11		Me	52.024	1	Arg57
D18		Ph	55.399	1	Glu140
D19		Ph	66.544	2	Glu131, Arg57
D20		Ph	56.726	2	Glu131, Arg136
D21		Ph	53.094	2	Arg57, Glu131
D22		Ph	57.503	1	Arg57
NMS-P937			72.696	3	Glu140, Lys61, Cys67

was redocked with the co-crystallized ligand NMS-P937 of Plk1 (2YAC) and with a reference molecule GW843682X. The dataset ligands and the designed molecules were docked into the active site of Plk1. The docking results of dataset ligands are shown in Table 6. The binding mode of the most active and least active compounds is shown in Fig. 4.

3.3. Binding mode analysis of most active and least active compounds

Fig. 4a, explains the docking analysis of the compound 32 with active site of 2YAC. The 3-amino group of the benzimidazole ring shows interaction with Lys82 (H-bond distance 2.2071 Å),

the carboxamide group of C=O with Cys133 (H-bond distance 2.1016 Å) and the amino group with Glu133 (H-bond distance 1.79103 Å). Fig. 4b represents the binding analysis of the least inactive compound 30, wherein the 3-amino group of benzimidazole ring interacts with Cys133 (H-bond distance 2.1258 Å), carboxyl group of (C=O), (C–OH) showing interaction with Lys82 (H-bond distance 1.6731 Å) and Asp194 (H-bond distance 2.1857 Å) respectively and amine group of thiazole ring showing interactions with Cys67 (H-bond distance 2.3242 Å). As described earlier, even though compound 30 showed good hydrogen interactions and docking score when compared to compound 32, it became the most inactive because of the absence of substituted electron withdrawing groups on thiazole and benzimidazole rings. Thus the presence of substituted electron withdrawing groups on thiophene and benzimidazole rings affords the Plk1 inhibitory potential of compound 32.

After detailed analysis of the 3D-QSAR models and the docking results, we identified the structural requirements that are necessary for molecules in the inhibition of Plk1 activity (Fig. 5). Further, the molecules were modified to enhance the inhibitory activity against Plk1 protein. Hence, we substituted electron withdrawing groups and hydrophobic features on the newly designed molecules, which show satisfactory docking results when compared to the dataset molecules, and the docking results are shown in Table 7.

4. Conclusions

The main aim of this study is to understand the salient structural features of selective Plk1 inhibitors, which will be useful for further design of novel effective Plk1 inhibitors. PHASE was used for the development of pharmacophore models and an atom-based 3D-QSAR model developed based on pharmacophore-based alignment. Pharmacophore studies reveal that two hydrogen bond acceptors, one hydrogen bond donor and two aromatic rings are the essential significant features for ligand binding, analyzed by docking studies where these features show good interactions with amino acids Cys133, Asp194, Glu131, Lys82, and Glu140 and also show further interactions with hydrophobic residues Cys67, Leu59 and Arg136 in the binding site of Plk1. Visual representation of the 3D-QSAR model explains the structural activity relationship, the influence of electron withdrawing, hydrophobic and H-donor features of molecular structure on Plk1 inhibition. The newly designed molecules based on these hydrophobic and electron withdrawing features also show better binding interactions with the active and hydrophobic residues of the Plk1 active domain. The combination of these molecular modeling results will provide the information required for better understanding of structural features necessary for biological interaction and are expected to be useful for further design of novel active Plk1 inhibitors.

Declaration of interest

The authors report no declarations of interest.

Acknowledgement

The authors are thankful to Dr. Vadivelan Sankaran, Associate Principal Scientist, GVK BIO Sciences Pvt. Ltd., India, for providing facilities to carry out the work.

References

- [1] D.M. Glover, I.M. Hagan, A.A. Tavares, Polo-like kinases: a team that plays throughout mitosis, *Genes. Dev.* 12 (1998) 3777–3787.
- [2] J.A. Winkles, G.F. Alberts, Differential regulation of Polo-like kinase 1, 2, 3, and 4 gene expression in mammalian cells and tissues, *Oncogene* 24 (2005) 260–266.
- [3] D.M. Lowery, D. Lim, M.B. Yaffe, Structure and function of Polo-like kinases, *Oncogene* 24 (2005) 248–259.
- [4] G. de Carcer, B. Escobar, A.M. Higuero, L. Garcia, A. Anson, G. Perez, M. Mollejo, G. Manning, B. Melendez, J. Abad-Rodriguez, M. Malumbres, Plk5, a Polo box domain-only protein with specific roles in neuron differentiation and glioblastoma suppression, *Mol. Cell. Biol.* 31 (2011) 1225–1239.
- [5] Y. Degenhardt, T. Lampkin, Targeting Polo-like kinase in cancer therapy, *Clin. Cancer Res.* 16 (2010) 384–389.
- [6] T.L. Schmit, M.C. Ledesma, N. Ahmad, Modulating Polo-like kinase 1 as a means for cancer chemoprevention, *Pharm. Res.* 27 (2010) 989–998.
- [7] L.Y. Lu, J.L. Wood, K. Minter-Dykhouse, L. Ye, T.L. Saunders, X. Yu, J. Che, Polo-like kinase 1 is essential for early embryonic development and tumor suppression, *Mol. Cell. Biol.* 28 (2008) 6870–6876.
- [8] Y.H. Kang, C.H. Park, T.S. Kim, N.K. Soung, J.K. Bang, B.Y. Kim, J.E. Park, K.S. Lee, Mammalian Polo-like kinase 1-dependent regulation of the PBIP1-CENP-Q complex at kinetochores, *J. Biol. Chem.* 286 (2011) 19744–19757.
- [9] J.R. Bader, J.M. Kasuboski, M. Winding, P.S. Vaughan, E.H. Hinchcliffe, K.T. Vaughan, Polo-like kinase1 is required for recruitment of dynein to kinetochores during mitosis, *J. Biol. Chem.* 286 (2011) 20769–20777.
- [10] M.A. van Vugt, B.C. van de Weerd, G. Vader, H. Janssen, J. Calafat, R. Klompmaier, R.M. Wolthuis, R.H. Medema, Polo-like kinase-1 is required for bipolar spindle formation but is dispensable for anaphase promoting complex/Cdc20 activation and initiation of cytokinesis, *J. Biol. Chem.* 279 (2004) 36841–36854.
- [11] R.F. Lera, M.E. Burkard, High mitotic activity of Polo-like kinase 1 is required for chromosome segregation and genomic integrity in human epithelial cells, *J. Biol. Chem.* 287 (2012) 42812–42825.
- [12] I.M. Brennan, U. Peters, T.M. Kapoor, A.F. Straight, Polo-like kinase controls vertebrate spindle elongation and cytokinesis, *PLoS One* 2 (2007) e409.
- [13] V. Archambault, D.M. Glover, Polo-like kinases: conservation and divergence in their functions and regulation, *Nat. Rev. Mol. Cell Biol.* 10 (2009) 265–275.
- [14] B. Song, X.S. Liu, X. Liu, Polo-like kinase 1 (Plk1): an unexpected player in DNA replication, *Cell Div.* 7 (2012) 1–7.
- [15] H.A. Lane, E.A. Nigg, Antibody microinjection reveals an essential role for human Polo-like kinase 1 (Plk1) in the functional maturation of mitotic centrosomes, *J. Cell Biol.* 135 (1996) 1701–1713.
- [16] I. Sumara, E. Vorlauffer, P.T. Stukenberg, O. Kelm, N. Redemann, E.A. Nigg, J.M. Peters, The dissociation of cohesin from chromosomes in prophase is regulated by Polo-like kinase, *Mol. Cell* 9 (2002) 515–525.
- [17] M. Glotzer, The molecular requirements for cytokinesis, *Science* 307 (2005) 1735–1739.
- [18] X. Liu, R.L. Erikson, Polo-like kinase (Plk)1 depletion induces apoptosis in cancer cells, *Proc. Natl. Acad. Sci. U.S.A.* 100 (2003) 5789–5794.
- [19] B. Spankuch-Schmitt, J. Bereiter-Hahn, M. Kaufmann, K. Strebhardt, Effect of RNA silencing of polo-like kinase-1 (PLK1) on apoptosis and spindle formation in human cancer cells, *J. Natl. Cancer Inst.* 94 (2002) 1863–1877.

- [20] Y.D. Yao, T.M. Sun, S.Y. Huang, S. Dou, L. Lin, J.N. Chen, J.B. Ruan, C.Q. Mao, F.Y. Yu, M.S. Zeng, J.Y. Zang, Q. Liu, F.X. Su, P. Zhang, J. Lieberman, J. Wang, E. Song, Targeted delivery of PLK1-siRNA by ScFv suppresses Her2+ breast cancer growth and metastasis, *Sci. Transl. Med.* 4 (2012) 130ra48.
- [21] W. Weichert, C. Denkert, M. Schmidt, V. Gekeler, G. Wolf, M. Kobel, M. Dietel, S. Hauptmann, Polo-like kinase isoform expression is a prognostic factor in ovarian carcinoma, *Br. J. Cancer* 90 (2004) 815–821.
- [22] X.S. Liu, B. Song, B.D. Elzey, T.L. Ratliff, S.F. Konieczny, L. Cheng, N. Ahmad, X. Liu, Polo-like kinase 1 facilitates loss of pten tumor suppressor-induced prostate cancer formation, *J. Biol. Chem.* 286 (2011) 35795–35800.
- [23] W. Weichert, G. Kristiansen, M. Schmidt, V. Gekeler, A. Noske, S. Niesporek, M. Dietel, C. Denkert, Polo-like kinase 1 expression is a prognostic factor in human colon cancer, *World J. Gastroenterol.* 11 (2005) 5644–5650.
- [24] F. Rodel, S. Keppner, G. Capalbo, R. Bashary, M. Kaufmann, C. Rodel, K. Strebhardt, B. Spankuch, Polo-like kinase 1 as predictive marker and therapeutic target for radiotherapy in rectal cancer, *Am. J. Pathol.* 177 (2010) 918–929.
- [25] J. Wagenblast, D. Hirth, L. Thron, C. Arnoldner, M. Diensthuber, T. Stöver, M. Hambek, Effects of the Polo-like-kinase-1-inhibitor BI2536 in squamous cell carcinoma cell lines of the head and neck, *Oncol. Lett.* 4 (2012) 175–177.
- [26] L. Chenzhong, Y. RiSheng, Diversity evolution and jump of Polo-like kinase 1 inhibitors, *Sci. China Chem.* 56 (2013) 1392–1401.
- [27] K. Strebhardt, Multifaceted Polo-like kinases: drug targets and antitargets for cancer therapy, *Nat. Rev. Drug Discov.* 9 (2010) 643–660.
- [28] T. Ikezoe, J. Yang, C. Nishioka, Y. Takezaki, T. Tasaka, K. Togitani, H.P. Koeffler, A. Yokoyama, A novel treatment strategy targeting Polo-like kinase 1 in hematological malignancies, *Leukemia* 23 (2009) 1564–1576.
- [29] M. Nihal, N. Stutz, T. Schmit, N. Ahmad, G.S. Wood, Polo-like kinase 1 (Plk1) is expressed by cutaneous T-cell lymphomas (CTCLs) and its downregulation promotes cell cycle arrest and apoptosis, *Cell Cycle* 10 (2011) 1303–1311.
- [30] K. Spaniol, J. Boos, C. Lanvers-Kaminsky, An in-vitro evaluation of the Polo-like kinase inhibitor GW843682X against paediatric malignancies, *Anticancer Drugs* 22 (2011) 531–542.
- [31] H.Y. Wang, Z.X. Cao, L.L. Li, P.D. Jiang, Y.L. Zhao, S.D. Luo, L. Yang, Y.Q. Wei, S.Y. Yang, Pharmacophore modeling and virtual screening for designing potential PLK1 inhibitors, *Bioorg. Med. Chem. Lett.* 18 (2008) 4972–4977.
- [32] S. Lu, H.C. Liu, Y.D. Chen, H.L. Yuan, S.L. Sun, Y.P. Gao, P. Yang, L. Zhang, T. Lu, Combined pharmacophore modeling, docking, and 3D-QSAR studies of PLK1 inhibitors, *Int. J. Mol. Sci.* 12 (2011) 8713–8739.
- [33] S.L. Dixon, A.M. Smondryev, E.H. Knoll, S.N. Rao, D.E. Shaw, R.A. Friesner, PHASE: a new engine for pharmacophore perception, 3D QSAR model development, and 3D database screening: 1. Methodology and preliminary results, *J. Comput. Aided Mol. Des.* 20 (2006) 647–671.
- [34] K.A. Emmittle, G.M. Adjebang, C.W. Andrews, J.G. Alberti, R. Bambal, S.D. Chamberlain, R.G. Davis-Ward, H.D. Dickson, D.F. Hassler, K.R. Hornberger, J.R. Jackson, K.W. Kuntz, T.J. Lansing, R.A. Mook Jr., K.E. Nailor, M.A. Pobanz, S.C. Smith, C.M. Sung, M. Cheung, Design of potent thiophene inhibitors of Polo-like kinase 1 with improved solubility and reduced protein binding, *Bioorg. Med. Chem. Lett.* 19 (2009) 1694–1697.
- [35] T.R. Rheault, K.H. Donaldson, J.G. Badiang-Alberti, R.G. Davis-Ward, C.W. Andrews, R. Bambal, J.R. Jackson, M. Cheung, Heteroaryl-linked 5-(1H-benzimidazol-1-yl)-2-thiophenecarboxamides: potent inhibitors of Polo-like kinase 1 (PLK1) with improved drug-like properties, *Bioorg. Med. Chem. Lett.* 20 (2010) 4587–4592.
- [36] Y. Sato, Y. Onozaki, T. Sugimoto, H. Kurihara, K. Kamijo, C. Kadowaki, T. Tsujino, A. Watanabe, S. Otsuki, M. Mitsuya, M. Iida, K. Haze, T. Machida, Y. Nakatsuru, H. Komatani, H. Kotani, Y. Iwasawa, Imidazopyridine derivatives as potent and selective Polo-like kinase (PLK) inhibitors, *Bioorg. Med. Chem. Lett.* 19 (2009) 4673–4678.
- [37] X.J. Chu, J. Cai, S. Chen, Y. Chen, J.R. Goodnow, Robert Alan, K. Le, K.C. Luk, S.G. Mischke, P.M. Wovkulich, Thiazolyl-benzimidazoles. US Patent 0160308 (2010).
- [38] F. Nader, G. Paul, J.R. Goodnow, Robert Alan, K. Le, C. Michoud, B.J. Fredrick, C. Jianping, 4-phenyl-thiazole-5-carboxylic acids and 4-phenyl-thiazole-5-carboxylic acid amides as plk1 inhibitors. WO Patent 096315 (2007).
- [39] LigPrep., version 2.3, 2009. Schrödinger, LLC, New York, NY, USA.
- [40] MacroModel., version 9.7, 2009. Schrödinger, LLC, New York, NY, USA.
- [41] F. Bai, X. Liu, J. Li, H. Zhang, H. Jiang, X. Wang, H. Li, Bioactive conformational generation of small molecules: a comparative analysis between force-field and multiple empirical criteria based methods, *BMC Bioinformatics* 11 (2010) 1–11.
- [42] PHASE, version 3.1, 2009. Schrödinger, LLC, New York, NY, USA.
- [43] A.M. Almerico, M. Tutone, A. Lauria, 3D-QSAR pharmacophore modeling and in silico screening of new Bcl-xl inhibitors, *Eur. J. Med. Chem.* 450 (2010) 4774–4782.
- [44] I. Beria, R.T. Bossi, M.G. Brasca, M. Caruso, W. Ceccarelli, G. Fachin, M. Fasolini, B. Forte, F. Fiorentini, E. Pesenti, D. Pezzetta, H. Poster, A. Scolaro, S. Re Depaolini, B. Valsasina, NMS-P937, a 4, 5-dihydro-1H-pyrazolo[4, 3-h]quinazoline derivative as potent and selective Polo-like kinase 1 inhibitor, *Bioorg. Med. Chem. Lett.* 21 (2011) 2969–2974.
- [45] Discovery Studio version 2.5, 2009. Accelrys, San Diego, California, USA.